NeuroImage 202 (2019) 116147

Contents lists available at ScienceDirect

NeuroImage

journal homepage: www.elsevier.com/locate/neuroimage

Task-based fMRI of a free-viewing visuo-saccadic network in the marmoset monkey

David J. Schaeffer [a], Kyle M. Gilbert [a], Yuki Hori [a], Lauren K. Hayrynen [a], Kevin D. Johnston [b], Joseph S. Gati [a], Ravi S. Menon [a,b], Stefan Everling [a,b,*]

[a] Centre for Functional and Metabolic Mapping, Robarts Research Institute, University of Western Ontario, London, Ontario, Canada
[b] Department of Physiology and Pharmacology, University of Western Ontario, London, Ontario, Canada

ARTICLE INFO

Keywords:
Common marmoset
Functional magnetic resonance imaging
Saccadic network

ABSTRACT

Saccadic tasks are often used to index aberrations of cognitive function in patient populations, with several neuropsychiatric and neurologic disorders characterized by saccadic dysfunction. The common marmoset (*Callithrix jacchus*) has received recent attention as an additional primate model for studying the neural basis of these dysfunctions – marmosets are amenable to a host of genetic manipulation techniques and have a lissencephalic cortex, which is well suited for a variety of recording techniques (e.g., calcium imaging, laminar electrophysiology). Because the marmoset cortex is mostly lissencephalic, however, the locations of frontal saccade-related regions (e.g., frontal eye fields (FEF)) are less readily identified than in Old World macaque monkeys. Further, although high quality histology-based atlases do exist for marmosets, identifying these regions based on histology alone is not always accurate, with the cytoarchitectonic boundaries often inconsonant with functional boundaries. As such, there is a need to map the functional location of these regions directly. Task-based functional magnetic resonance imaging (fMRI) is of utility in this regard, allowing for detection of whole-brain signal changes in response to moving stimuli. Here, we conducted task-based fMRI in marmosets at ultra-high field (9.4 T) during a free-viewing visuo-saccadic task. We also conducted the same task in humans at ultra-high field (7 T) to validate that our simple task was indeed evoking the visuo-saccadic circuitry we expected (as defined by a meta-analysis of fMRI saccade studies). In the marmosets, we found that the task evoked a robust visuo-saccadic topology, with visual cortex (V1, V2, V3, V4) activation extending ventrally to MT, MST, FST and dorsally into V6, 19M, 23V. This topology also included putative cingulate eye field (area 32 and 24d), posterior parietal cortex (with strongest activation in lateral intraparietal area (LIP)), and a frontolateral peak in area 8 aV in marmosets, extending into 45, 46, 8aD, 6DR, 8c, 6 aV, 6DC. Overall, these results support the view that marmosets are a promising preclinical modelling species for studying saccadic dysfunction related to neuropsychiatric or neurodegenerative human brain diseases.

1. Introduction

Saccadic eye movement tasks are often used to index aberrations of cognitive function in patient populations, with several neuropsychiatric and neurologic disorders characterized by saccadic dysfunction (e.g., schizophrenia, Parkinson's; Fukushima et al., 1988, 1994; Everling and Fischer, 1998; Mcdowell et al., 2002; McDowell et al., 2008). The saccadic network is among the most broadly studied cortical networks in non-human primate models, with a wealth of electrophysiological, histochemical tracing, and magnetic resonance imaging (MRI) evidence suggesting comparable networks between humans and macaques (see Johnston and Everling, 2008, for review). In the burgeoning New World marmoset (*Callithrix jacchus*) model, however, there is a relative paucity of evidence mapping functional saccadic network topologies (albeit, electrically evoked saccades in marmoset frontal cortex were reported in the early 20th century; Mott et al., 1909). Given the similarities between the marmoset visual system and the human visual system (e.g., color vision, high visual acuity, the ability to foveate; Mitchell et al., 2014; Mitchell and Leopold, 2015; Nakamura et al., 2018; Solomon and Rosa, 2014), marmosets have recently been touted as a powerful model for visual neuroscience. Systematic and detailed mapping of the marmoset visual system has been documented over the past three decades (Bourne

* Corresponding author. Robarts Research Institute, University of Western Ontario, London, Ontario, Canada.
E-mail addresses: dschaeff@uwo.ca (D.J. Schaeffer), severling@uwo.ca (S. Everling).

https://doi.org/10.1016/j.neuroimage.2019.116147
Received 1 May 2019; Received in revised form 22 August 2019; Accepted 29 August 2019
Available online 31 August 2019

et al., 2002; Burman et al., 2006; Elston et al., 1999; Elston and Rosa, 2006; Fritsches and Rosa, 1996; Lui et al., 2006; Palmer and Rosa, 2006; Rosa et al., 2009, 1997; Rosa and Elston, 1998; Rosa and Schmid, 1995; Rosa and Tweedale, 2000), but task-based whole-brain accounts related to marmoset saccadic eye movements have still yet to be documented. With clear evidence that marmosets can be trained to perform visual tasks (Johnston et al., 2018; Mitchell et al., 2014; Nakamura et al., 2018), functional magnetic resonance imaging (fMRI) is of utility in this regard, allowing for detection of whole-brain signal changes in response to moving visual stimuli. Here, we collected task-based fMRI while marmosets (at 9.4 T) and humans (at 7 T) performed a simple block design free-viewing visuo-saccadic task.

Because the marmoset cortex is mostly lissencephalic, the locations of frontal saccade-related regions (e.g., frontal eye fields (FEF)) are less readily identified than in other primate species – macaques, for example, have sulcal landmarks allowing for localization of FEF, with this region located in the anterior bank of the arcuate sulcus (Bruce et al., 1985; Schall, 1991, 2002; Stanton et al., 1988). Moreover, although high quality histology-based atlases do exist for marmosets (e.g., Paxinos et al., 2012), identifying these regions based on histology alone is not always accurate – we have recently demonstrated that the cytoarchitectonic boundaries of marmoset frontal cortex may not map directly to functional boundaries (Schaeffer et al., 2019a, 2019b). As such, mapping the function of these regions directly can be useful for validating the location of the regions with reference to known cytoarchitectonic delineations in stereotactic space (Paxinos et al., 2012). In that vein, we sought to clarify the location of the FEF in the marmoset using task-based fMRI. Initial evidence for the location of FEF in marmosets came from microstimulation of frontal cortex, eliciting various types of eye movements in both areas 6 and 8 (both dorsal and ventral portions; Blum et al., 1982). The putative location of FEF in marmosets is also evidenced by recent electrophysiological recordings demonstrating alpha oscillations in preparation for eye movements in area 8aD (Johnston et al., 2019), a location consistent with recent whole-brain resting state fMRI seed analyses in anesthetized marmosets (Ghahremani et al., 2017; Schaeffer et al., 2019b). A task-based fMRI study in marmosets (Hung et al., 2015) also hinted at the location of FEF in marmosets (see Fig. 3E and F therein) wherein marmosets were viewing static visual stimuli, (15° ±5° visual angle).

Here, we leveraged recent advances in hardware development for awake marmoset imaging (Schaeffer et al., 2019c) at ultra-high field (9.4 T) to collect nearly motionless fMRI in three adult male marmosets while they performed a simple free-viewing visuo-saccade task. Our aim was to implement a task-based fMRI paradigm that would allow for localization of visuo-saccadic circuitry with little to no training demand – in doing so, we could elicit a robust response from this circuity in an otherwise naïve animal in as quickly as a single 60 min fMRI session. To that end, we employed a block-design task that consisted of action movie trailers (appearing at different visual eccentricities), providing robust visual stimulation and eliciting stimulus-driven eye movements. We also conducted the same task in two humans at ultra-high field (7 T) to validate that the task was eliciting the circuitry that we expected (i.e., compared to known human saccadic circuitry), as shown by meta-analysis.

2. Methods

2.1. Subjects

2.1.1. Marmosets

At 9.4 T, data were collected from three male marmosets (*Callithrix jacchus*), weighing 380 g (marmoset 1), 245 g (marmoset 2), and 360 g (marmoset 3). Marmosets were 36, 19, and 20 months, respectively, at the time of the experiment. Experimental procedures were in accordance with the Canadian Council of Animal Care policy and a protocol approved by the Animal Care Committee of the University of Western Ontario Council on Animal Care. All animal experiments complied with the ARRIVE guidelines.

2.1.2. Humans

At 7 T, data were acquired on two adult male human subjects (aged 32 and 37 years). Humans subjects provided informed consent and were screened for MRI contraindications. Data was collected in accordance with and approved by the Human Subjects Research Ethics Board at the University of Western Ontario. All imaging (both species) was performed at the Centre for Functional and Metabolic Mapping at the University of Western Ontario.

2.2. Marmoset surgical implantation and head-fixation training

All three marmosets underwent an aseptic surgical procedure to implant an MRI-compatible head chamber. The purpose of the chamber was to fix the head and thereby prevent animal motion during MRI acquisition. The chamber implantation procedure is described in detail in Johnston et al. (2018) and Schaeffer et al. (2019c); in brief, several coats of adhesive resin (All-bond Universal, Bisco, Schaumburg, Illinois, USA) were applied using a microbrush, air dried, and cured with an ultraviolet dental curing light (King Dental). Then, a two-component dental cement (C & B Cement, Bisco, Schaumburg, Illinois, USA) was applied to the skull and to the bottom of the chamber, which was then lowered onto the skull via a stereotactic manipulator to ensure correct location and orientation. The chamber was 3D printed at 0.25 mm resolution using stereolithography and a clear photopolymer resin (Clear Resin V4; Form 2, Formlabs, Somerville, Massachusetts, USA).

Before MRI acquisition, the marmosets were first acclimatized to the head-fixation system and a mock MRI environment (including sequence sounds; see Schaeffer et al., 2019c for open-source hardware designs for the animal holder and detailed training procedures). Each marmoset was acclimatized over the course of three weeks prior to imaging. The marmosets were not trained on the free-viewing saccade task *per se*, as described in the next section.

2.3. Free-viewing visuo-saccadic task and eye tracking

For marmosets, a block design was used in which nine baseline blocks (16.5 s each) were alternated with eight task blocks (16.5 s each; see Fig. 1). During baseline blocks, a 0.36° circular gray cue was displayed in the center of the screen against a black background – this was in part to be used as a fixation point (although marmosets did not fixate *per se*), but also as a source of light that served to mitigate visual nystagmus invoked by the high magnetic field. During task blocks, the dot disappeared and action movie trailers (1.54° height x 2.26° width) were presented to the left or right of the center at 2.75° above center, 0° from center, or 2.75° below center (i.e., 6 different locations total). On odd trial blocks (marked large in Fig. 1), the videos were shown 4.32° to the left or right of center and on even blocks (marked small in Fig. 1) the videos were shown 0.96° from center. As such, on the odd blocks, the distance between the center of the videos was 7.56° and on even blocks, the distance was 1.68°. The videos switched locations every second during the block – the same video clips (and position orders) were used for odd and even blocks. The marmosets were rewarded at the start and end of every block (i.e., every 16.5 s) to keep the animal awake and engaged. The liquid reward (diluted sweetened condensed milk) was delivered via injection pump (Model NE-510, New Era Pump Systems, Inc., Farmingdale, New York, USA). The reward volume was set to 50 μL per dispense and was delivered over the course of 1 s; note that reward tube was placed outside of the marmosets mouth (~5 mm away) and thus they need to extend their tongue in order to lick the reward from the tube. The maximum reward volume received (i.e., if all of the reward deliveries were licked) was 2.4 ml over the course of three task runs. For humans, the same task and parameters were used, with slightly different block timing (14 s baseline blocks and 15 s task blocks). The humans scanned for this study are authors of the manuscript (and designed the task) – as such, no task

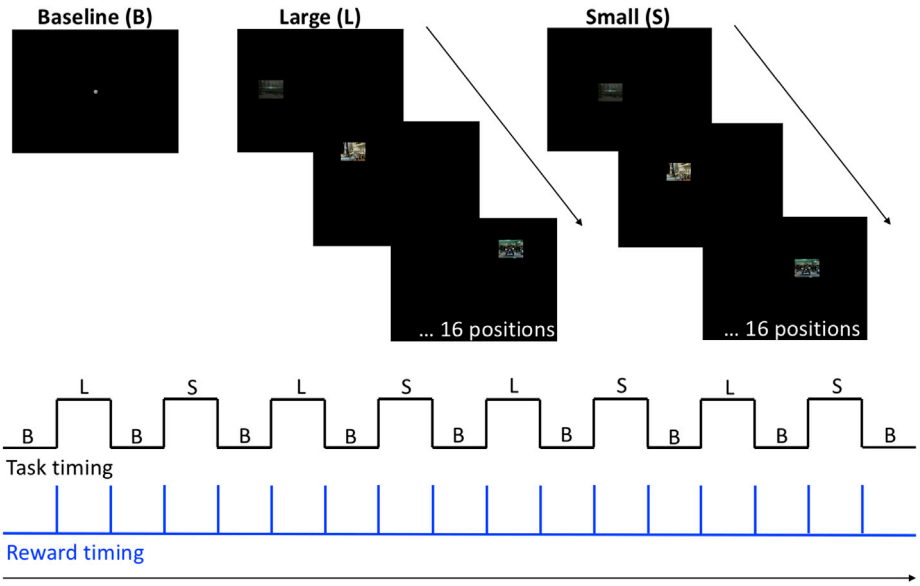

Fig. 1. Stimuli and experimental design for task fMRI. Top shows the stimuli for the baseline (B) condition and the task conditions, including the large (L) and small (S) conditions. During both task conditions, video clips (action movie trailers) appeared at different visual eccentricities (7.56° apart for L and 1.68° for S, 16 positions for each). The black line below the stimuli shows the task condition order and the blue line shows the reward timing with reference to the task.

instructions were given before the human imaging sessions.

For the marmosets, the stimuli were presented via projector (Model VLP-FE40, Sony Corporation, Tokyo, Japan), reflected off of a first surface mirror, and back-projected the image onto a plastic screen that was velcroed to the front of the scanner bore. For the humans, the stimuli were presented via a rear projection system (Avotech SV-6011, Avotec Incorporated, Stuart, Florida, USA) off of a first surface mirror system affixed to the head coil. For both species, the stimuli were presented via Keynote (Version 7.1.3, Apple Incorporated, California, USA), with the stimulus timing (based on a per TR transistor-transistor logic (TTL) pulse) achieved using a Raspberry Pi (Model 3 B+, Raspberry Pi Foundation, Cambridge, UK) programmed in-house.

For the marmosets, an MRI-compatible camera (Model 12M-i, MRC Systems GmbH, Heidelberg, Germany) with a 60 Hz sampling rate was affixed the front of the animal holder allowing for tracking of the eye position. These signals were digitized and recorded using an ISCAN ETL-200 system (ISCAN, Incorporated, Woburn, Massachusetts, USA). The X and Y position information was processed using in-house MATLAB scripts (The Mathworks, Matick, MA). Specifically, eye blinks were removed and the data was smoothed using a median filter, and eye position densities were quantified to verify that the marmosets were indeed watching the stimuli as they appeared (see Fig. 2 for representative plots). Eye tracking was not conducted in humans.

2.4. Image acquisition: marmosets

2.4.1. Animal holder and MRI hardware

An integrated animal holder and 5-channel radiofrequency receive array was used to rigidly fix the head chamber to the receive coil. This hardware was designed in-house and is described in detailed in Schaeffer et al. (2019c), wherein the open-source computer-aided design files are linked. The animal holder was designed to first restrain the animal with neck and tail plates (in the sphinx position), then for quick and efficient head-fixation through the use of hinged clamps. The MRI-compatible camera (described above) allowed for continuous monitoring by a veterinary technician for any sign of struggle or discomfort. Given that skull-attached chambers are generally accompanied by magnetic-susceptibility image artifacts (via differences in the magnetic susceptibility between the chamber, adhesive, air, and tissue, as well as the surgical displacement of the skin, fat, and muscle), we sought to ameliorate this distortion by filling the chamber with a water-based lubricant gel (MUKO SM321N, Canadian Custom Packaging Company, Toronto, Ontario, Canada) prior to each imaging session.

Data were acquired using an 9.4 T 31 cm horizontal bore magnet (Varian/Agilent, Yarnton, UK) and Bruker BioSpec Avance III console with the software package Paravision-6 (Bruker BioSpin Corp, Billerica, MA), a custom-built high-performance 15-cm-diameter gradient coil with 400-mT/m maximum gradient strength (xMR, London, CAN; Peterson et al., 2018), and the receive coil described above. Radiofrequency transmission was accomplished with a quadrature birdcage coil (12-cm inner diameter) built in-house.

2.4.2. Imaging parameters

Functional imaging was performed over multiple sessions (days) for each animal, with six task-based functional runs (at 187 vol each) per animal with the following parameters: TR = 1500 ms, TE = 15 ms, flip angle = 40°, field of view = 64 × 64 mm, matrix size = 128 × 128, voxel size = 0.5 × 0.5 × 0.5 mm, slices = 42, bandwidth = 500 kHz, GRAPPA acceleration factor: 2 (anterior-posterior). Six resting state runs with the same parameters (but with 600 volumes) were acquired for marmosets one and two. T2-weighted structural scans were acquired for each animal during one of the awake sessions with the following parameters: TR = 5500 ms, TE = 53 ms, field of view = 51.2 × 51.2 mm, matrix size = 384 × 384, voxel size = 0.133 × 0.133 × 0.5 mm, slices = 42, bandwidth = 50 kHz, GRAPPA acceleration factor: 2.

2.5. Image acquisition: humans

Data was collected using a 68 cm head-only 7 T MRI scanner (Siemens Magnetom Step 2.3, Erlangen, Germany) equipped with an AC-84 Mark II head gradient coil. Radiofrequency signaling was accomplished with an in-house 8-channel parallel transmit and 32-channel receive coil (Gilbert et al., 2015).

2.5.1. Imaging parameters

Functional imaging was performed during a single session for each human, with 3 functional runs (at 255 vol each) per person with the following parameters: TR = 1000 ms, TE = 20 ms, flip angle = 30°, field of view = 208 × 208 mm, matrix size = 104 × 104, voxel

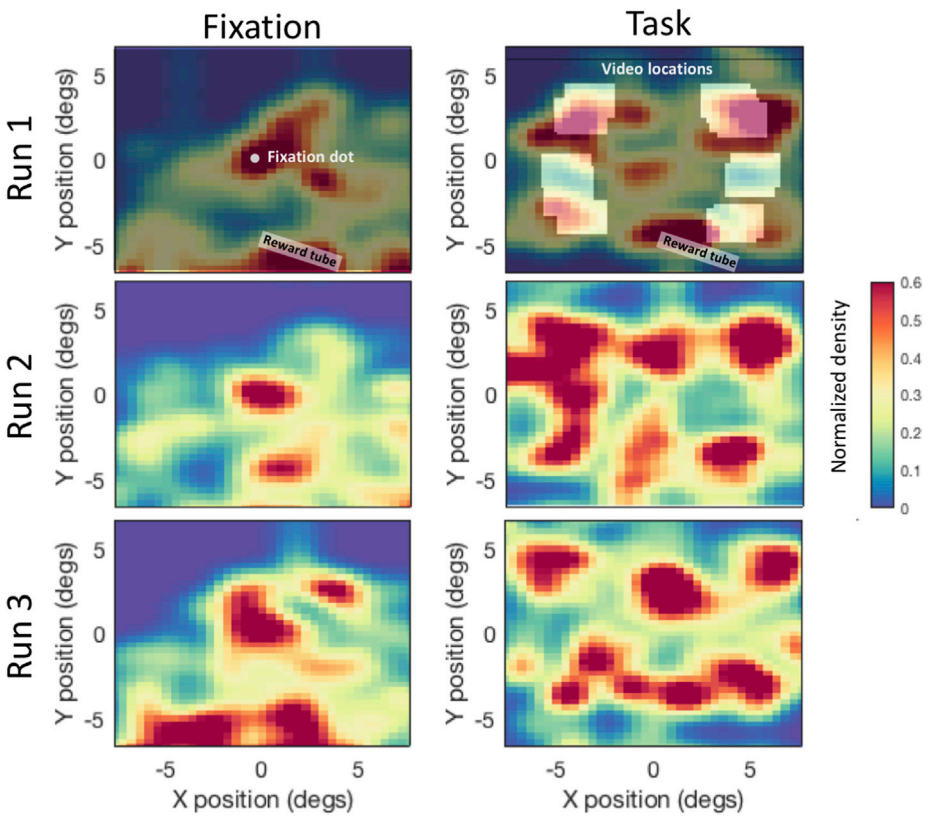

Fig. 2. Density histogram of eye positions during fixation and task (large condition). Plots show density histograms of eye positions (marmoset 3: runs 1–3) during the baseline (fixation) condition (left panel) and same for eye positions during the task (large condition blocks only; right panel). The first run shows the stimuli overlaid on the histograms, with the fixation dot (left panel) and the locations of the video clips (right panel). As seen in both the baseline (fixation) and task conditions, the marmosets also looked at the reward tube, which was just above their mouth. Eye tracking was not performed in humans.

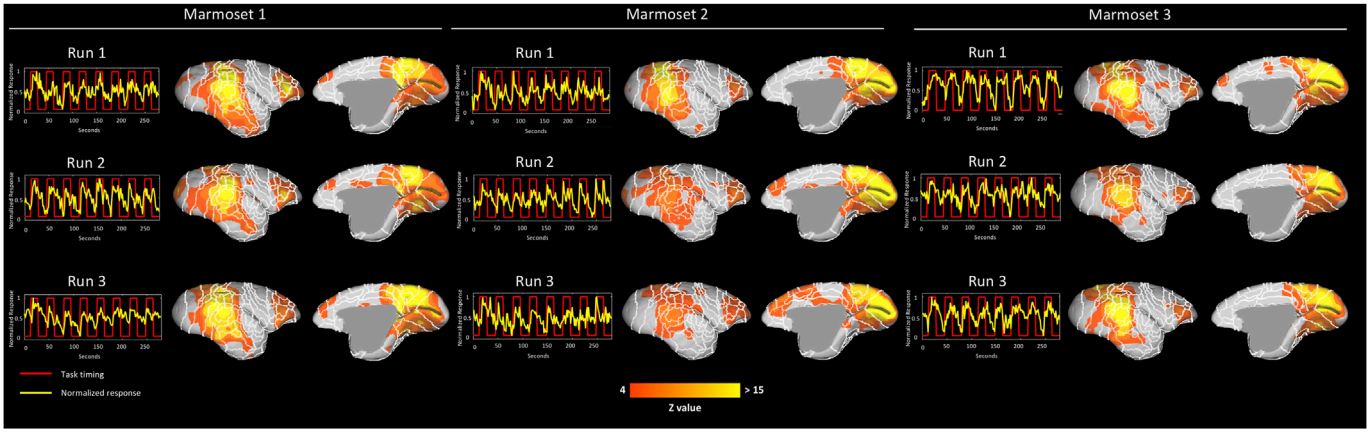

Fig. 3. Marmoset task-based patterns derived using hybrid ICA. For each marmoset, task timing (red line) and normalized BOLD response (yellow line) are to the left of the associated patterns of activation for each run. Patterns of activation (Z values) are on the NIH marmoset brain template surface (Liu et al., 2018). Medial and lateral surfaces of the right hemisphere are shown. Cytoarchitectonic boundary labels are shown in white, with labels for each region shown in Supplemental Fig. 1.

size = 2 × 2 × 2 mm, slices = 63, bandwidth = 140 Hz/Px, GRAPPA acceleration factor: 3 (anterior-posterior). MP2RAGE structural scans were acquired for each person with the following parameters: TR = 6000 ms, TE = 2.83 ms, field of view = 240 × 240 mm, matrix size = 320 × 320, voxel size = 0.75 × 0.75 × 0.75 mm, bandwidth = 140 Hz/Px.

2.6. Image preprocessing

For both species, fMRI data preprocessing was the same, unless otherwise noted. The data was preprocessed using AFNI (Cox, 1996) and FSL (Smith et al., 2004). Raw functional images were converted to NifTI format using dcm2niix (Li et al., 2016) and reoriented from the sphinx position using FSL (marmosets only). The images were then despiked (AFNI's 3dDespike) and volume registered to the middle volume (AFNI's 3dvolreg). The motion parameters from volume registration were stored for later use with nuisance regression. Images were smoothed by a 1.5 mm (marmosets) and 4 mm (humans) full-width at half-maximum Gaussian kernel to reduce noise (AFNI's 3dmerge). An average functional image was then calculated for each session and registered (FSL's FLIRT) to each animal's T2-weighted image (MP2RAGE, in humans) – the 4D time series data was carried over using this transformation matrix. Anatomical images were manually skull-stripped and this mask was applied to the functional images in anatomical space. Marmoset T2-weighted and human MP2RAGE images were then non-linearly registered to the NIH marmoset brain atlas (Liu et al., 2018) and the MNI152 template (Montreal Neurological Institute, McGill University, Montreal, Quebec, Canada), respectively, using Advanced Normalization Tools (ANTs; Avants et al., 2011) and the resultant transformation

matrices stored for later transformation (see below). The olfactory bulb was manually removed from the marmoset T2-weighted images of each animal prior to registration, as it was not included in the template image.

2.7. Task-based topologies

To circumvent the collinearity of the licking/reward circuity and the visuo-saccadic circuity (see timing in Fig. 1) in the marmosets, we employed a hybrid independent component analysis (ICA) design (Mckeown, 2000; Schaeffer et al., 2013) – this analysis allowed us to identify separate spatial components for the two circuitries, then use those time courses as stimulus regressors in a single model. For both marmosets and humans, FSL's MELODIC (Beckmann and Smith, 2004) was applied to each run separately, with 50 dimensions for both species. Each component set was manually inspected – in the marmosets, a task component and licking component was identified for each run based on the time course frequency, at 0.03 Hz (task) and 0.06 Hz (licking/reward). Similarly, in humans the task component was identified at a frequency of 0.034 Hz.

The time courses derived from the ICA analysis were then used in a regression analysis (AFNI's 3dDeconvolve) for each run. For the marmosets, both a task component and a licking/reward component were entered into the same model, along with polynomial (N = 5) detrending regressors, bandpass regressors, and the motion parameters derived from the volume registration described above (albeit the marmoset imaging sessions had little to no motion; see Schaeffer et al., 2019c for further details). In humans, the regression analysis was identical, but with one less stimulus regressor (i.e., no licking/reward component in humans). To protect against false positives, a clustering method derived from Monte Carlo simulations was applied to the individual maps, in both species (using AFNI's AlphaSim). The resultant regression coefficient maps were then registered to the respective template spaces using the transformation matrices described above and then converted to Z value maps. The individual animal/run Z value maps were then projected to surface space with CARET (Van Essen et al., 2001); for the marmosets, a surface-based version of the volume template was generously provided by the authors of the NIH marmoset brain template (Liu et al., 2018). Group functional connectivity maps were also calculated for each species (AFNI's 3dttest++) and projected onto surface space.

2.8. Meta-analysis of human saccade topologies

Given that our task was not a canonical saccadic eye movement task (e.g., a prosaccade task), *per se,* we conducted a meta-analysis of human saccade studies to determine how our task-evoked topologies compared to previous "saccade" fMRI studies. In doing so, we could delineate the regions related to the saccadic circuitry from other regions related to the additional stimulation from the video clips. To do this, we employed the automated meta-analysis technique described in Yarkoni et al. (2011). Explicitly, we searched the word "saccade" on the Neurosynth.org website, yielding a meta-analysis of 79 studies preferential related to the term "saccade" (see Yarkoni et al., 2011 for details). We then downloaded this map and transformed in to surface space in CARET (Van Essen et al., 2001) for comparison with our task-evoked map.

2.9. Resting-state seed analysis

Because the functional location of FEF has yet to be thoroughly validated in the marmoset, we sought to corroborate the location of this region with a second fMRI analysis. Using the RS-fMRI acquired from two of the marmosets (marmoset 1 and 2), we calculated seed-based connectivity across the brain using two separate seeds: one in area MT, and another in the superior colliculus (both bilateral, as defined in the NIH template atlas (Liu et al., 2018)). Both of these regions are well known to be directly anatomically connected with FEF in the macaque brain (Fries, 1984; Komatsu and Suzuki, 1985; Leichnetz, 1981; Rodman et al., 1990). As such, by calculating seed maps, we could compare the task-free functional connectivity of these regions with the maps elicited from our free-viewing visuo-saccadic task in the same animals. The preprocessing steps described above were also used for the RS-fMRI seed analysis, apart from the task regressors. Instead, the mean time courses from MT and SC were used as the regressors, for each run. As described above, these resultant maps were transformed into surface space and converted to Z values.

3. Results

3.1. Task-based topologies

Using a hybrid-ICA analysis, we derived task and licking/reward related networks from each fMRI run for all three marmosets. As shown in Fig. 3, the BOLD response associated with the ICA-derived task components overlapped well with the task timing, as did the component identified as the licking/reward network (Fig. 4 for individual runs). Further, when those time courses were subjected to a regression analysis, there was a robust visuo-saccadic network shown across all three marmosets and in both humans (Fig. 3, marmosets; Fig. 5), humans).

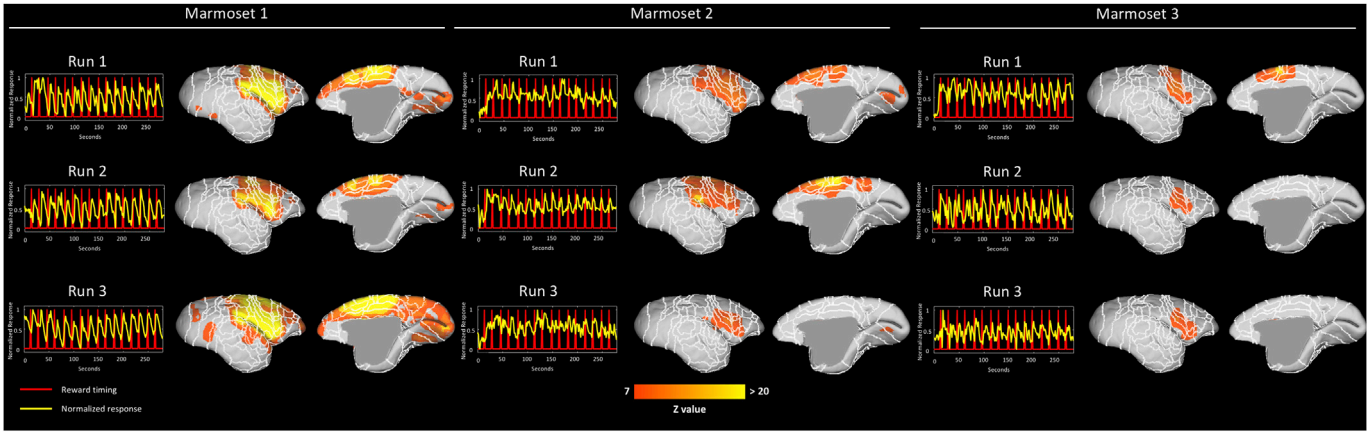

Fig. 4. Marmoset licking/reward-based patterns derived using hybrid ICA. For each marmoset, reward timing (red line) and normalized BOLD response (yellow line) are to the left of the associated patterns of activation for each run. Patterns of activation (Z values) are on the NIH marmoset brain template surface (Liu et al., 2018). Medial and lateral surfaces of the right hemisphere are shown. Cytoarchitectonic boundary labels are shown in white, with labels for each region shown in Supplemental Fig. 1.

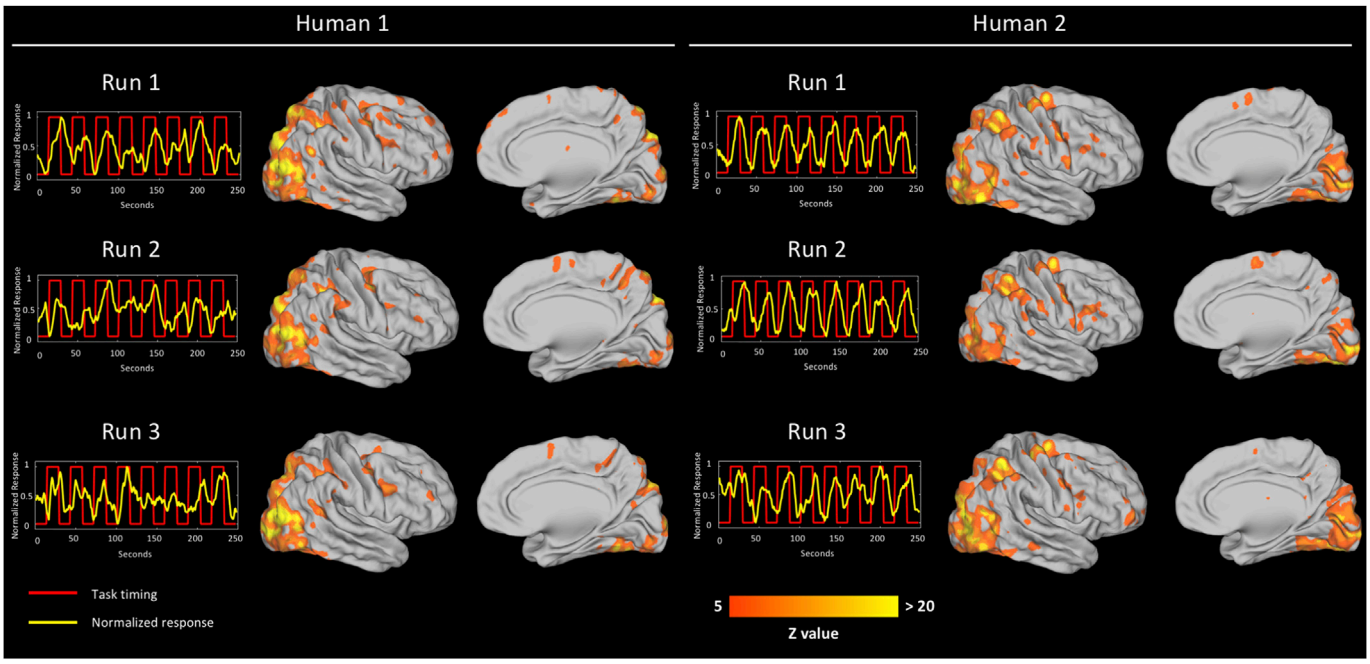

Fig. 5. Human task-based patterns derived using hybrid ICA. For each person, task timing (red line) and normalized BOLD response (yellow line) are to the left of the associated patterns of activation for each run. Patterns of activation (Z values) are on the MNI template surface. Medial and lateral surfaces of the right hemisphere are shown.

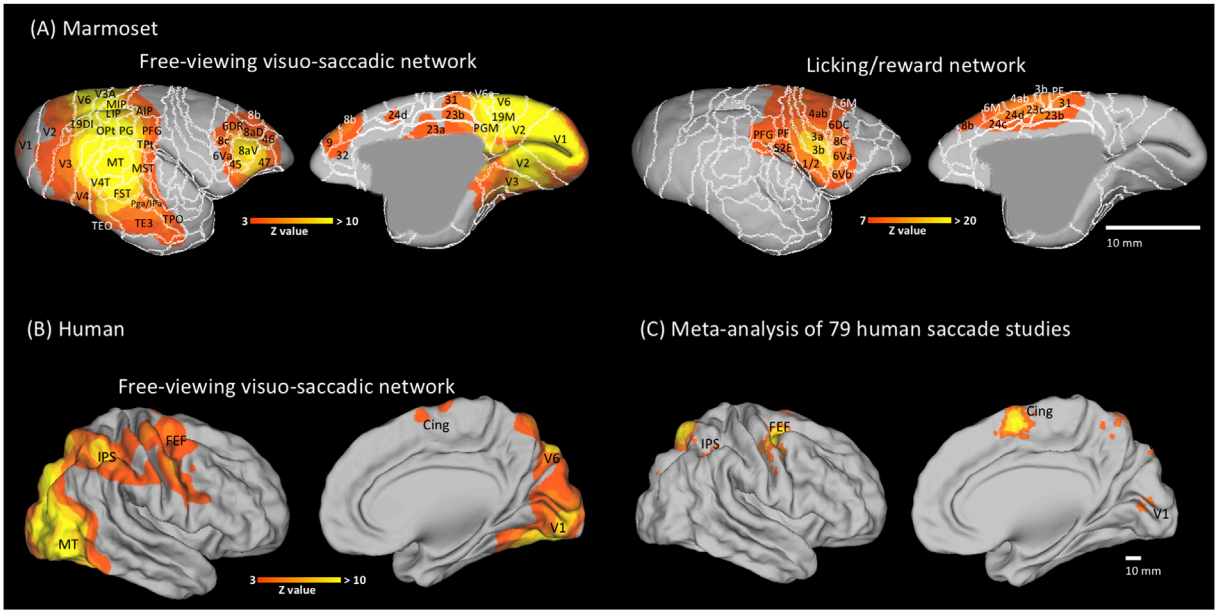

Fig. 6. Group maps for marmosets and humans. (A) Marmoset group maps for the free-viewing visuo-saccadic task (left) and licking/reward network (right). White lines show cytoarchitectonic boundaries, with the relevant regions labelled in black. (B) Human group map for the visuo-saccadic network. Medial and lateral surfaces of the right hemisphere are shown. (C) Meta-analysis of human fMRI studies conducted using the term "saccade" via Neurosynth.org. IPS = intraparietal sulcus; FEF = frontal eye fields; cing = cingulate cortex.

3.1.1. Marmoset group maps

The marmoset group map is shown in Fig. 6A; the visuo-saccadic task evoked strong activation along the medial surface of V1 that extended into area V2 (both dorsally and ventrally on the medial surface). Ventromedially, strong activation was also shown in area V3, extending into area V4, TEO, and TH and dorsomedially in area V6, 19M, 23V that extended to posterior cingulate (i.e., the border of A31, 23b, 23a). More anteriorly, however, peaks in activation were present in area 24d, 8b, and area 9 – these middle and anterior cingulate areas could correspond to the putative 'cingulate eye field' in the marmoset.

The free-viewing visuo-saccadic task also activated a vast network across the lateral brain surface. The lateral surface of areas V1 and V2 showed relatively little activation, but it is important to note that the signal-to-noise ratio in visual cortex was relatively weak compared to the rest of the brain (as shown in Schaeffer et al., 2019c, Fig. 4F). This is likely due to the magnetic susceptibility at the back of the head and concomitant geometric distortion that was worsened by the accelerated fMRI sequence. Accordingly, areas V1 and V2 were likely activated in the posterior half of the visual cortex of the marmosets, but that activation was simply not detected amid the weak/noisy signal. Ventrolaterally,

where the signal was sufficiently high, areas V3, 19DI, V4, V4T were activated, with the strongest activation in area MT (V5) that extended into MST, FST, PGa/IPa, TEO and TE3 (see especially peak in anterior TE3). Dorsolaterally, the task evoked activation across posterior parietal cortex (OPt, PG, PFG, MIP, VIP, LIP, AIP, and PEC) with the strongest activation in the posterior LIP. In lateral prefrontal cortex, there was a strong peak in area 8 aV that extended into the surrounding areas (45, 46, 8aD, 6DR, 8c, 6 aV, 6DC).

The group map of the licking/reward network (Fig. 6A, right panel) was quite discrete from that evoked by the task. This activation was much stronger than the task-associated network (thus a higher Z value threshold, Fig. 6). Along the medial surface, relatively strong activation was elicited across middle and posterior cingulate regions (23b, 31, 3b, 23c, 24d and c) and extended into area 6m and 8b. Along the lateral surface, activation was shown across a large network including TP, PF, SE1 and 2, PE, 1/2, 3b, 2a, 4 ab, 4c, 45a, 6Va. 8C, and 6DC. The strongest peak was in area 3a and 3b – this is consistent with microsimulation in marmosets eliciting jaw, lip, and check movements in this "face" region (see Burish et al., 2008, Figs. 2–5 therein).

3.1.2. Human group maps

In the human subjects, the hybrid-ICA analysis yielded a robust visuo-saccadic network in both subjects. Specifically, as shown in the group map (Fig. 6b), strong activation was shown ventromedially along area V1, V2, V3, V4, and V5 and dorsomedially in area V6, then strong another peak in the cingulate eye field. On the lateral surface, the humans showed a larger extent of activation along the surface of visual cortex (V1, V2, V3, V4, and V5) than the marmosets, but as noted above, the coil design for the marmosets prohibited strong signal acquisition in that area, and thus any comparison of these regions across species would be tenuous. The human group map also showed a peak in intra-parietal sulcus (IPS), which is consistent with the region activation for canonical saccade tasks (see meta-analysis below). The human group map showed activation along both sides of the central sulcus, which was not shown in marmosets (albeit see the peak along precentral sulcus shown in the metanalysis below). This effect, however, is likely a function of having a low threshold (i.e., that used in both humans and marmosets for comparability); with a higher SNR, the effect size in the humans led to more extensive activation at the same threshold. As expected with a visuo-saccadic task, there was a strong peak in FEF. It is important to note that human FEF and primate FEF (i.e., macaque) differ cytoarchitectonically, with the human FEF functional peak lying in area 6 and macaque FEF in area 8 (Koyama et al., 2004) – the present results along with recent microsimulation in marmosets (Selvanayagam et al., 2019) suggest that marmoset FEF also lies in area 8. Determining how these patterns compare to other human studies employing saccade tasks allowed us to 1) test if our task evoked peak activations in what is typically shown to be "saccade-related" areas and 2) suggest what additional regions were associated with the videos used in our task (as opposed to static stimuli). To that end, we conducted a meta-analysis described below.

3.2. Meta-analysis of human saccade topologies

To determine how our task-evoked topologies compared to previous "saccade" fMRI studies, we conducted a meta-analysis of 79 human fMRI saccade studies. As shown in Fig. 6C, this analysis yielded a circuitry remarkably similar to that evoked with our task (Fig. 6B), with the exception of visual cortex. These results can also be compared to a separate meta-analysis of prosaccade-only fMRI studies conducted by Zhou and Shu (2017). From both the Zhou and Shu (2017) meta-analysis and the present one, it is clear that our task evoked additional circuity (i.e., that not related to saccades). This activation, however, was prescribed to visual cortex and the ventral visual stream (e.g., strong Brodmann area 17, 18, 19, 37, and 39 activation in our task). Accordingly, it is important to note that our task may not be strictly considered a "saccadic" task (thus referred to as visuo-saccadic), as additional regions were evoked by the presentation of the videos. That being said, however, IPS, cingulate eye field, and FEF peaks were consistent between the meta-analysis and the group map from our free-viewing visuo-saccadic task (see Fig. 6B and C).

3.3. Resting-state seed analysis

In addition to task-based fMRI, we also collected RS-fMRI in two of the marmosets with the purpose of comparing seed-based connectivity in areas known to be connected to FEF (Komatsu and Suzuki, 1985; Rodman et al., 1990) with the location of FEF derived from our task-based design. Seed-based analyses in both area MT and SC yielded circuitry similar to that found with the saccade task. Specifically, both the MT and SC seed analysis yielded peaks in the ventro-lateral portion of area 8 aV, which is consistent with the peak location of putative FEF identified for the task based analysis (see Fig. 7). Interestingly, both regions also showed a medial peak in area 8aD/6DR. We have shown this same medial pattern

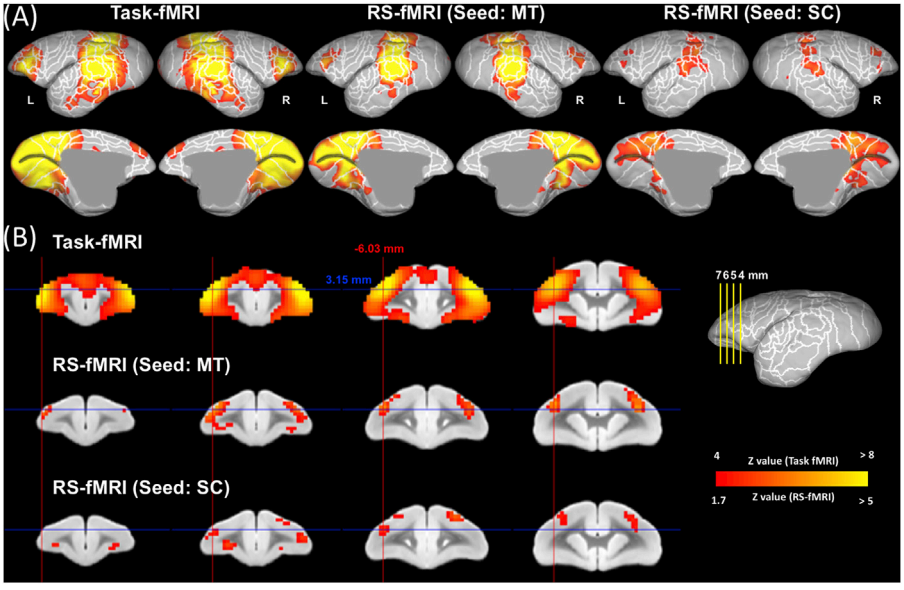

Fig. 7. Comparison of task-based pattern in marmosets to seed based RS-fMRI maps. (A) Left: the group task-based visuo-saccadic network on left and right marmoset brain surfaces. Middle: the result of seed-based regression across the brain with time courses extracted from area MT. Right: the result of seed-based regression across the brain with time courses extracted from superior colliculus (SC). (B) The same maps as above, but shown across four selected slices. Blue and red crosshairs reference Z and X stereotactic position, respectively, across slices. The surface to the right of the slices shows the stereotactic Y positions relative to the interaural plane, with cytoarchitectonic delineations shown in white.

before with RS-fMRI based seed analyses in marmosets (Ghahremani et al., 2017), but the behavioral correlates of this region require further investigation.

4. Discussion

In this study we sought to demonstrate that marmosets can indeed perform a visuo-saccadic task in the fMRI environment, and in turn, map these whole brain topologies for the first time in marmosets. To do so, we employed a block-design task that consisted of action movie trailers (appearing at different visual eccentricities), providing robust visual stimulation and eliciting stimulus-driven eye movements. We then used a hybrid-ICA analysis to delineate the visuo-saccadic circuity from reward/licking circuitry in the marmoset data, and also employed the same hybrid-ICA analysis in the humans to extract the saccadic network. Overall, we found a robust visuo-saccadic network in the both species, showing peaks of activation in posterior parietal cortex, area MT, FEF, and cingulate eye fields (putative in marmosets). Both species also showed an extensive pattern on visual cortex activation in response to our visuo-saccadic task, but our SNR in the marmoset data was not optimal due to limitations in our coil design. Our results serve to clarify the functional location of marmoset FEF, which to date has been suggested to exist somewhere in the vicinity of 8 aV and 8aD (Ghahremani et al., 2017; Johnston et al., 2019), or even as posterior as area 6, bordering primary motor cortex (Krubitzer and Kaas, 1990). Based on our task, we suggest that the FEF region (at least that associated with small-amplitude eye movements) is located in area 8 aV, which is consistent with recent microsimulation in marmosets from our group (Selvanayagam et al., 2019). Overall, our results suggest that the marmoset is a viable nonhuman primate comparator of human visuo-saccadic circuitry, showing similar network topologies.

With the aim to elicit saccadic circuitry in both marmosets and humans, we chose to use a relatively simple, salient visual task that required little to no training demand for the marmosets, and would not lead to confounds due to comprehension (i.e., the human subjects understanding an explicit set of instructions not communicable to the marmosets). Indeed, the task allowed us to elicit robust responses from the marmoset visuo-saccadic circuity in otherwise naïve animals in as little as a single ~5 min fMRI session (Fig. 3). From the meta-analysis of other saccade fMRI studies in humans (Fig. 6C), it is clear that the saccadic network is robustly evoked with this task in both species. As stated above, however, it is important to note that our task evoked additional regions across visual cortex and the ventral visual stream – these regions were likely related to the presentation of the videos and thus not "saccadic" regions, *per se*.

A major difference between the marmoset and human imaging sessions was that we needed to reward the marmosets (at the start and end of every block) to keep the animals engaged in the task. This comes with the caveat that the marmosets licking/reward circuity was coactivated during both the task blocks and the fixation period. To circumvent the collinearity of the licking/reward circuity and the visuo-saccadic, we employed a hybrid ICA design – this analysis allowed us to identify separate spatial components for the two circuitries, then use those time courses as stimulus regressors in a single model. As shown in Fig. 6A, the visuo-saccadic task evoked strong activation along the medial surface of V1 that extended into area V2 (both dorsally and ventrally on the medial surface). Ventromedially, strong activation was also shown in area V3, extending into area V4 and TEO. Weaker activation was present in area TH, but given that there was not a clear a peak in this area, the activation here was likely a threshold dependent effect exacerbated by spatial smoothing. Dorsomedially, the task elicited activation in area V6, 19M, 23V that extended to posterior cingulate (i.e., the border of A31, 23b, 23a). Although there was activation in posterior cingulate, no peaks were found here and thus we hesitate to make any definitive statements that the task activated these areas, *per se* (again, likely threshold and smoothing dependent). More anteriorly, however, peaks in activation were present in area 24d, 8b, and area 9 – this is consistent with our previous report (Schaeffer et al., 2019b, Fig. 4b) showing RS-fMRI connectivity between what is likely FEF (i.e., 8 aV) and 24d, 9, and 32. These middle and anterior cingulate areas could correspond to the putative 'cingulate eye field' in the marmoset, although this assertion remains to be more thoroughly tested. As previously reported (Schaeffer et al., 2019b), these cingulate peaks can be differentiated from those correlated with dorsal and ventral 4 ab (i.e., 'motor cingulate') in a way similar to that found in humans (Paus, 2001).

The free-viewing visuo-saccadic task also activated a vast network across the lateral brain surface. The lateral surface of areas V1 and V2 showed relatively little activation, but it is important to note that the signal-to-noise ratio in visual cortex was relatively weak compared to the rest of the brain (as shown in Schaeffer et al., 2019c, Fig. 4F). Ventrolaterally, where the signal was sufficiently high, areas V3, 19DI, V4, V4T were activated, with the strongest activation in area MT (V5) that extended into MST, FST, PGa/IPa, TEO and TE3 (see especially peak in anterior TE3). This pattern along the ventral visual stream is consistent with a previous task-based fMRI study in marmosets (Hung et al., 2015; see Fig. 3e, therein) where natural objects (faces and objects) were presented in a block design. Dorsolaterally, the task evoked activation across posterior parietal cortex (OPt, PG, PFG, MIP, VIP, LIP, AIP, and PEC) with the strongest activation in the posterior LIP. This pattern can be contrasted against patterns evoked by static visual stimuli in the Hung et al. (2015) study, which showed little parietal activation. As such, it is likely that the strong pattern of parietal activity here was associated with the moving stimuli in our task. In lateral prefrontal cortex, there was a strong peak in area 8 aV that extended into the surrounding areas (45, 46, 8aD, 6DR, 8c, 6 aV, 6DC) – this is consistent with microsimulation we have conducted in marmosets, where smaller amplitude saccades are evoked along the border of 8 aV and 45 (Selvanayagam et al., 2019). Given the relatively small eccentricity of the stimuli in our task (7.56° maximum), the peak location is consistent with the lateral 8 aV location where smaller amplitude saccades are evoked.

Given that the functional location of FEF in marmosets has been reported in several, quite distant areas, this study serves to clarify the location of FEF in the marmoset. That being said, we recognize that our task was not a saccadic eye movement task *per se*, and that the humans were fixating on the central fixation dot and consciously making goal directed eye movements, whereas the marmosets were performing the task more passively (i.e., only making less eye movements during fixation, but not truly fixating; see Fig. 2 for gaze heat map from marmoset 3; eye tracking was not performed in humans). As such, we also conducted a second level of validation with RS-fMRI data from both species (i.e., completely independent of task), by placing seeds in superior colliculus and area MT, two regions known to have structural connectivity with FEF in macaque monkeys (Komatsu and Suzuki, 1985; Rodman et al., 1990). The resting state maps seeded from both area superior colliculus and area MT yielded connectivity to the FEF loci identified by the task. Interestingly, the connectivity from both regions also extended into areas 8aD and 6DR, consistent with our previous estimation of the location of FEF (Ghahremani et al., 2017; Johnston et al., 2019; Schaeffer et al., 2019a). We aver that this more medial location is likely related to larger amplitude eye movements and also head movements (similar to medial FEF in both humans and macaques; Bruce et al., 1985; Corneil et al., 2010; Robinson and Fuchs, 2017) – we have recently corroborated this with microsimulation in marmosets (Selvanayagam et al., 2019). We did initially design our task to elicit both large and small eye movements (large: odd blocks; small: even blocks), but because of the physical limitations of the visual angle imposed by our 9.4 T bore, the maximum visual angle of eye movements with our task was still only 7.56°. Given the maps of the small and large amplitude block regressors yield very similar results, our analysis combined both blocks. Accordingly, our localization of FEF in marmosets with the saccade task should be taken with the caveat that it was elicited with relatively small amplitude eye movements.

Overall, our results demonstrate that a free-viewing visuo-saccadic network can be reliably elicited in marmosets during task-based fMRI acquisition. These results suggest that the marmoset could indeed be a viable preclinical model for saccadic dysfunction. Although it remains to be demonstrated that marmosets can perform more cognitively complex oculomotor tasks (e.g., antisaccade tasks) in the MRI environment, this prospect is likely with recent demonstrations that marmosets can perform such tasks while head-fixed in the upright position (Johnston et al., 2019). With the available genetic manipulation techniques, publicly available anatomical tracer data (Majka et al., 2016), and host of other neuroimaging techniques being developed for marmosets (e.g, calcium imaging (Kondo et al., 2017; Sadakane et al., 2015)), the marmoset model is poised to make major contributions to visual neuroscience both at the basic mechanistic level and as a preclinical model for human neuropsychiatric disorders.

Author notes

Support was provided by the Canadian Institutes of Health Research (FRN 148365) and the Canada First Research Excellence Fund to BrainsCAN. We wish to thank Miranda Bellyou for animal preparation and care and Dr. Alex Li for scanning assistance.

Appendix A. Supplementary data

Supplementary data to this article can be found online at https://doi.org/10.1016/j.neuroimage.2019.116147.

References

Avants, B.B., Tustison, N.J., Song, G., Cook, P.A., Klein, A., Gee, J.C., 2011. A reproducible evaluation of ANTs similarity metric performance in brain image registration. Neuroimage 54, 2033–2044. https://doi.org/10.1016/j.neuroimage.2010.09.025.

Beckmann, C.F., Smith, S.M., 2004. Probabilistic independent component analysis for functional magnetic resonance imaging. IEEE Trans. Med. Imaging 23, 137–152. https://doi.org/10.1109/TMI.2003.822821.

Blum, B., Kulikowski, J.J., Carden, D., Harwood, D., 1982. Eye movements induced by electrical stimulation of the frontal eye fields of marmosets and squirrel monkeys. Brain Behav. Evol. 21, 34–41. https://doi.org/10.1159/000121613.

Bourne, J.A., Tweedale, R., Rosa, M.G.P., 2002. Physiological responses of new world monkey V1 neurons to stimuli defined by coherent motion. Cerebr. Cortex 12, 1132–1145.

Bruce, C.J., Goldberg, M.E., Bushnell, M.C., Stanton, G.B., 1985. Primate frontal eye fields. II. Physiological and anatomical correlates of electrically evoked eye movements. J. Neurophysiol. 54, 714–734.

Burish, M.J., Stepniewska, I., Kass, J.H., 2008. Microstimulation and architectonics of frontoparietal cortex in common marmosets (Callithrix jacchus). J Comp Neurol. 507, 1151–1168. https://doi.org/10.1002/cne.

Burman, K.J., Palmer, S.M., Gamberini, M., Rosa, M.G.P., 2006. Cytoarchitectonic subdivisions of the dorsolateral frontal cortex of the marmoset monkey (Callithrix jacchus), and their projections to dorsal visual areas. J. Comp. Neurol. 495, 149–172. https://doi.org/10.1002/cne.20837.

Corneil, B.D., Elsley, J.K., Nagy, B., Cushing, S.L., 2010. Motor output evoked by subsaccadic stimulation of primate frontal eye fields. Proc. Natl. Acad. Sci. 107, 6070–6075. https://doi.org/10.1073/pnas.0911902107.

Cox, R.W., 1996. AFNI: software for analysis and visualization of functional magnetic resonance neuroimages. Comput. Biomed. Res. 29, 162–173. https://doi.org/10.1006/cbmr.1996.0014.

Elston, G.N., Rosa, M.G.P., 2006. Ipsilateral corticocortical projections to the primary and middle temporal visual areas of the primate cerebral cortex : area-specific variations in the morphology of connectionally identified pyramidal cells. Eur. J. Neurosci. 23, 3337–3345. https://doi.org/10.1111/j.1460-9568.2006.04847.x.

Elston, G.N., Tweedale, R., Rosa, M.G.P., 1999. Cellular heterogeneity in cerebral cortex: a study of the morphology of pyramidal neurones in visual areas of the marmoset monkey. J. Comp. Neurol. 415, 33–51. https://doi.org/10.1002/(SICI)1096-9861(19991206)415:1%3c33::AID-CNE3%3e3.0.CO;2-M.

Everling, S., Fischer, B., 1998. The antisaccade: a review of basic research and clinical studies. Neuropsychologia 36, 885–899. https://doi.org/10.1016/S0028-3932(98)00020-7.

Fries, W., 1984. Cortical projections to the superior colliculus in the macaque monkey: a retrograde study using horseradish peroxidase. J. Comp. Neurol. 230, 55–76. https://doi.org/10.1002/cne.902300106.

Fritsches, K.A., Rosa, M.G.P., 1996. Visuotopic organisation of striate cortex in the marmoset monkey (Callithrix jacchus). J. Comp. Neurol. 372, 264–282. https://doi.org/10.1002/(SICI)1096-9861(19960819)372:2%3c264::AID-CNE8%3e3.0.CO;2-1.

Fukushima, J., Fukushima, K., Chiba, T., Tanaka, S., Yamashita, I., Kato, M., 1988. Disturbances of voluntary control of saccadic eye movements in schizophrenic patients. Biol. Psychiatry 23, 670–677.

Fukushima, J., Fukushima, K., Miyasaka, K., Yamashita, I., 1994. Voluntary control of saccadic eye movement in patients with frontal cortical lesions and Parkinsonian patients in comparison with that in Schizophrenics. Biol. Psychiatry 36, 21–30. https://doi.org/10.1016/0006-3223(94)90058-2.

Ghahremani, M., Hutchison, R.M., Menon, R.S., Everling, S., 2017. Frontoparietal functional connectivity in the common marmoset. Cerebr. Cortex 27, 3890–3905. https://doi.org/10.1093/cercor/bhw198.

Gilbert, K., Gati, J., Kho, E., Klassen, M., Zeman, P., Menon, R., 2015. An parallel-transmit, parallel-receive coil for routine scanning on a 7T head-only scanner. In: Proceedings of the 23rd Annual Meeting of ISMRM, Toronto, Canada.

Hung, C.C., Yen, C.C., Ciuchta, J.L., Papoti, D., Bock, N.A., Leopold, D.A., Silva, A.C., 2015. Functional MRI of visual responses in the awake, behaving marmoset. Neuroimage 120, 1–11. https://doi.org/10.1016/j.neuroimage.2015.06.090.

Johnston, K., Everling, S., 2008. Neurophysiology and neuroanatomy of reflexive and voluntary saccades in non-human primates. Brain Cogn. 68, 271–283. https://doi.org/10.1016/j.bandc.2008.08.017.

Johnston, K., Ma, L., Schaeffer, L., Everling, S., 2019. Alpha-oscillations modulate preparatory activity in marmoset area 8Ad Alpha-oscillations modulate preparatory activity in marmoset area. J. Neurosci. 39, 1855–1866.

Johnston, K.D., Barker, K., Schaeffer, L., Schaeffer, D., Everling, S., 2018. Methods for chair restraint and training of the common marmoset on oculomotor tasks. J. Neurophysiol. 119. https://doi.org/10.1152/jn.00866.2017.

Komatsu, H., Suzuki, H., 1985. Projections from the functional subdivisions of the frontal eye field to the superior colliculus in the monkey. Brain Res. 327, 324–327. https://doi.org/10.1016/0006-8993(85)91528-8.

Kondo, M., Kobayashi, K., Ohkura, M., Nakai, J., Matsuzaki, M., 2017. Two-Photon calcium imaging of the medial prefrontal cortex and hippocampus without cortical invasion. Elife 6, 1–20. https://doi.org/10.7554/eLife.26839.

Koyama, M., Hasegawa, I., Osada, T., Adachi, Y., Nakahara, K., Miyashita, Y., 2004. Functional magnetic resonance imaging of macaque monkeys performing visually guided saccade tasks: comparison of cortical eye fields with humans. Neuron 41, 795–807.

Krubitzer, L.A., Kaas, J.H., 1990. Cortical connections of MT in four species of primates: areal, modular, and retinotopic patterns. Vis. Neurosci. 5, 165–204. https://doi.org/10.1017/S0952523800000213.

Leichnetz, G.R., 1981. The prefrontal cortico-oculomotor trajectories in the monkey. A possible explanation for the effects of stimulation/lesion experiments on eye movement. J. Neurol. Sci. 49, 387–396. https://doi.org/10.1016/0022-510X(81)90029-0.

Li, X., Morgan, P.S., Ashburner, J., Smith, J., Rorden, C., 2016. The first step for neuroimaging data analysis: DICOM to NIfTI conversion. J. Neurosci. Methods 264, 47–56. https://doi.org/10.1016/j.jneumeth.2016.03.001.

Liu, C., Ye, F.Q., Yen, C.C.C., Newman, J.D., Glen, D., Leopold, D.A., Silva, A.C., 2018. A digital 3D atlas of the marmoset brain based on multi-modal MRI. Neuroimage 169, 106–116. https://doi.org/10.1016/j.neuroimage.2017.12.004.

Lui, L.L., Bourne, J.A., Rosa, M.G.P., 2006. Functional Response Properties of Neurons in the Dorsomedial Visual Area of New World Monkeys (Callithrix jacchus). https://doi.org/10.1093/cercor/bhi094.

Majka, P., Chaplin, T.A., Yu, H.H., Tolpygo, A., Mitra, P.P., Wójcik, D.K., Rosa, M.G.P., 2016. Towards a comprehensive atlas of cortical connections in a primate brain: mapping tracer injection studies of the common marmoset into a reference digital template. J. Comp. Neurol. 524, 2161–2181. https://doi.org/10.1002/cne.24023.

Mcdowell, J.E., Brown, G.G., Paulus, M., Martinez, A., Stewart, S.E., Dubowitz, D.J., Braff, D.L., 2002. Neural correlates of refixation saccades and antisaccades in normal and schizophrenia subjects. Biol. Psychiatry 51, 216–223.

McDowell, J.E., Dyckman, K.A., Austin, B., Clementz, B.A., 2008. Neurophysiology and Neuroanatomy of reflexive and volitional saccades: evidence from studies of humans. J. Neurophysiol. 68, 255–270. https://doi.org/10.1016/j.bandc.2008.08.016. Neurophysiology.

Mckeown, M.J., 2000. Detection of consistently task-related activations in fMRI data with hybrid independent component analysis, Vol 35, pp. 24–35. https://doi.org/10.1006/nimg.1999.0518.

Mitchell, J.F., Leopold, D.A., 2015. The marmoset monkey as a model for visual neuroscience. Neurosci. Res. 93, 20–46. https://doi.org/10.1016/j.neures.2015.01.008.

Mitchell, J.F., Reynolds, J.H., Miller, C.T., 2014. Active vision in marmosets: a model system for visual neuroscience. J. Neurosci. 34, 1183–1194. https://doi.org/10.1523/jneurosci.3899-13.2014.

Mott, F., Shuster, E., Halliburton, W., 1909. Cortical lamination and localisation in the brain of the marmoset. Roy. Soc. Proc. B 80, 124–136.

Nakamura, K., Koba, R., Miwa, M., Yamaguchi, C., Suzuki, H., Takemoto, A., 2018. A method to train marmosets in visual working memory task and their performance. Front. Behav. Neurosci. 12, 1–9. https://doi.org/10.3389/fnbeh.2018.00046.

Palmer, S.M., Rosa, M.G.P., 2006. Quantitative analysis of the corticocortical projections to the middle temporal area in the marmoset Monkey : evolutionary and functional implications. Eur. J. Neurosci. 24, 2389–2405. https://doi.org/10.1093/cercor/bhj078.

Paus, T., 2001. Primate anterior cingulate cortex: where motor control, drive and congition interface. Nat Rev Neurosci. 2, 417–424. https://doi.org/10.1038/35077500.

Paxinos, G., Watson, C., Petrides, M., Rosa, M., Tokuno, H., 2012. The Marmoset Brain in Stereotaxic Coordinates. Academic Press.

Peterson, J., Chaddock, R., Dalrymple, B., Van Sas, F., Gilbert, K.M., Klassen, L.M., Gati, J.S., Handler, W.B., Chronik, B.A., 2018. Development of a gradient and shim insert system for marmoset imaging at 9.4 T. In: Proceedings of the 26th Annual Meeting ISMRM. Paris, France, p. 4421.

Robinson, D.A., Fuchs, A.F., 2017. Eye movements evoked by stimulation of frontal eye fields. J. Neurophysiol. 32, 637–648. https://doi.org/10.1152/jn.1969.32.5.637.

Rodman, H., Gross, C., Albright, T., 1990. Afferent basis of visual response properties in area MT of the macaque. II. Effects of superior colliculus removal. J. Neurosci. 10, 1154–1164. https://doi.org/10.1523/jneurosci.10-04-01154.1990.

Rosa, M.G.P., Elston, G.N., 1998. Visuotopic organisation and neuronal response selectivity for direction of motion in visual areas of the caudal temporal lobe of the marmoset monkey (Callithrix jacchus): middle temporal area, middle temporal crescent, and surrounding cortex. J. Comp. Neurol. 393, 505–527. https://doi.org/10.1002/(SICI)1096-9861(19980420)393:4%3c505::AID-CNE9%3e3.0.CO;2-4.

Rosa, M.G.P., Fritsches, K.A., Elston, G.U.Y.N., 1997. The second visual area in the marmoset Monkey : visuotopic organisation , magnification factors , architectonical boundaries , and modularity. J. Comparitive Neurol. 387, 547–567.

Rosa, M.G.P., Palmer, S.M., Gamberini, M., Burman, K.J., Yu, H., Reser, D.H., Bourne, J.A., Tweedale, R., Galletti, C., 2009. Connections of the dorsomedial visual Area : pathways for early integration of dorsal and ventral streams in extrastriate cortex. J. Neurosci. 29, 4548–4563. https://doi.org/10.1523/JNEUROSCI.0529-09.2009.

Rosa, M.G.P., Schmid, L.M., 1995. Visual areas in the dorsal and medial extrastriate cortices of the marmoset. J. Comp. Neurol. 359, 272–299. https://doi.org/10.1002/cne.903590207.

Rosa, M.G.P., Tweedale, R., 2000. Visual areas in lateral and ventral extrastriate cortices of the marmoset monkey. J Comparitive Neurol. 422, 621–651.

Sadakane, O., Watakabe, A., Ohtsuka, M., Takaji, M., Sasaki, T., Kasai, M., Isa, T., Kato, G., Nabekura, J., Mizukami, H., Ozawa, K., Kawasaki, H., Yamamori, T., 2015. In vivo two-photon imaging of dendritic spines in marmoset neocortex. eNeuro 2 e0019-15.2015.

Schaeffer, D.J., Amlung, M.T., Li, Q., Krafft, C.E., Austin, B.P., Dyckman, K.A., Mcdowell, J.E., 2013. Neural correlates of behavioral variation in healthy adults' antisaccade performance. Psychophysiology 50. https://doi.org/10.1111/psyp.12030.

Schaeffer, David J., Gilbert, K.M., Gati, J.S., Menon, R.S., Everling, S., 2019a. Intrinsic functional boundaries of lateral frontal cortex in the common marmoset monkey. J. Neurosci. 39, 1020–1029.

Schaeffer, David J., Gilbert, K.M., Ghahremani, M., Gati, J.S., Menon, R.S., Everling, S., 2019b. Intrinsic functional clustering of anterior cingulate cortex in the common marmoset. Neuroimage 186, 301–307. https://doi.org/10.1016/j.neuroimage.2018.11.005.

Schaeffer, David J., Gilbert, K.M., Hori, Y., Gati, J.S., Menon, R.S., Everling, S., 2019c. Integrated radiofrequency array and animal holder design for minimizing head motion during awake marmoset functional magnetic resonance imaging. Neuroimage 193, 126–138. https://doi.org/10.1016/j.neuroimage.2019.03.023.

Schall, J., 1991. Neuronal Activity elated to Visually Guided Saccades e Frontal Eye Fields s Monkeys . J. Neurophysiol. 66, 559–579.

Schall, J.D., 2002. The neural selection and control of saccades by the frontal eye field. Philos. Trans. R. Soc. Biol. Sci. 357, 1073–1082. https://doi.org/10.1098/rstb.2002.1098.

Selvanayagam, J., Johnston, K.D., Schaeffer, D.J., Hayrynen, L.K., Everling, S., 2019. Functional Localization of the Frontal Eye Fields in the Common Marmoset Using Microstimulation bioRxiv, 715359. https://doi.org/10.1101/715359.

Smith, S.M., Jenkinson, M., Woolrich, M.W., Beckmann, C.F., Behrens, T.E.J., Johansen-Berg, H., Bannister, P.R., De Luca, M., Drobnjak, I., Flitney, D.E., Niazy, R.K., Saunders, J., Vickers, J., Zhang, Y., De Stefano, N., Brady, J.M., Matthews, P.M., 2004. Advances in functional and structural MR image analysis and implementation as FSL. Neuroimage 23, S208–S219. https://doi.org/10.1016/j.neuroimage.2004.07.051.

Solomon, S.G., Rosa, M.G.P., 2014. A simpler primate brain: the visual system of the marmoset monkey. Front. Neural Circuits 8, 1–24. https://doi.org/10.3389/fncir.2014.00096.

Stanton, G.B., Goldberg, M.E., Bruce, C.J., 1988. Frontal eye field efferents in the macaque monkey: I. Subcortical pathways and topography of striatal and thalamic terminal fields. J. Comp. Neurol. 271, 473–492. https://doi.org/10.1002/cne.902710402.

Van Essen, D.C., Drury, H.A., Dickson, J., Harwell, J., Hanlon, D., Anderson, C.H., 2001. An integrated software suite for surface-based analyses of cerebral cortex. J. Am. Med. Inform. Assoc. 8, 443–459. https://doi.org/10.1136/jamia.2001.0080443.

Yarkoni, T., Poldrack, R.A., Nichols, T.E., Essen, D.C. Van, Wager, T.D., 2011. Large-scale Automated Synthesis of Human Functional Neuroimaging Data 8. https://doi.org/10.1038/NMETH.1635.

Zhou, W., Shu, H., 2017. A meta-analysis of functional magnetic resonance imaging studies of eye movements and visual word reading. Brain Behav. 7, e00683.